








Net 220 Gbps/ λ IM/DD Transmssion in O-Band and C-Band With Silicon Photonic Traveling-Wave MZM

Md Samiul Alam , *Graduate Student Member, IEEE*, Xueyang Li , *Graduate Student Member, IEEE*,
Maxime Jacques , Zhenping Xing , Alireza Samani , Eslam El-Fiky , Ping-Chiek Koh ,
and David V. Plant, *Fellow, IEEE*

Abstract—We present the design and characterization of O-band and C-band silicon photonic (SiP) traveling wave Mach-Zehnder modulators (TW-MZM) allowing 220 Gbps/ λ net rate operation. The designed modulators show over 45 GHz 3-dB E-O bandwidth with a single-segment design. In the O-band, with simple linear feed forward equalization, we transmit net 203 (200) Gbps signal over 2 km (10 km) of single-mode fiber (SMF) below the hard-decision forward error correction (HD-FEC) BER threshold of 3.8×10^{-3} . With the aid of nonlinear Volterra equalizer and one 2.3V_{pp} driving signal, we transmit net 225 (216) Gbps PAM8 signals assuming 20% overhead soft-decision FEC with a normalized general mutual information (NGMI) threshold of 0.8798 over 2 km (10 km) of SMF. The C-band design enables net 220 Gbps in B2B and net 215 Gbps over 500 m of SMF above the specified NGMI threshold. These results are the highest reported net rate for SiP MZM in an intensity modulation direct-detection (IM/DD) system, fabricated entirely in a commercial foundry.

Index Terms—Electrooptic modulators, intensity modulation, optical interconnections, Volterra equalization.

I. INTRODUCTION

THE EXPONENTIAL demand for high bandwidth applications is causing a rapid increase in data-center (DC) traffic, which is why cost-effective optical transceiver solutions are essential [1]. Since most of this traffic involves intra-datacenter and inter-datacenter links, intensity modulation / direct detection (IM/DD) schemes are utilized because of the cost-effectiveness and power efficiency. To keep pace with this growing demand,

Manuscript received January 14, 2021; revised March 13, 2021; accepted April 14, 2021. Date of publication April 19, 2021; date of current version July 2, 2021. (Md Samiul Alam and Xueyang Li contributed equally to this work.) (Corresponding author: Xueyang Li.)

Md Samiul Alam, Xueyang Li, Maxime Jacques, Zhenping Xing, Alireza Samani, and David V. Plant are with Photonic Systems Group, Department of Electrical and Computer Engineering, McGill University, Montréal, QC H3A 0E9, Canada (e-mail: md.samiul.alam@mail.mcgill.ca; xueyang.li@mail.mcgill.ca; maxime.jacques@mail.mcgill.ca; zhenping.xing@mail.mcgill.ca; alireza.samani@mail.mcgill.ca; david.plant@mcgill.ca).

Eslam El-Fiky is with Photonic Systems Group, Department of Electrical and Computer Engineering, McGill University, Montréal, QC H3A 0E9, Canada, and also with the Department of Electrical Engineering, Alexandria University, Alexandria 21544, Egypt (e-mail: eslam.elfiky@mail.mcgill.ca).

Ping-Chiek Koh is with Lumentum Corporation, San Jose, CA 95131 USA (e-mail: ping-chiek.koh@lumentum.com).

Color versions of one or more figures in this article are available at <https://doi.org/10.1109/JLT.2021.3074096>.

Digital Object Identifier 10.1109/JLT.2021.3074096

optical transceivers operating at high symbol rates and higher order modulation formats are being investigated. PAM4 has been adopted in IEEE 802.3bs standard for 400 GbE and a QSFP-DD800 MSA has started working to extend the capacity of QSFP-DD pluggable module form factor from 400 Gbps to 800 Gbps [2]–[3]. Though coherent is a strong contender for high-speed solution covering reach from 80 km and beyond, IM/DD solution will continue to dominate DR (datacenter reach for up to 500 m SMF), FR (fiber reach for up to 2 km SMF) and LR (long reach for up to 10 km SMF) transmission in the foreseeable future [3]. For the next generation Ethernet targeting 800 GbE and 1.6 TbE over short reach distances, 200 Gbps/ λ is thus an important milestone [4].

In recent years, several high-speed experimental works have been reported with Mach-Zehnder modulators (MZMs) and electro-absorption modulators with distributed feedback lasers (EA-DFB) [5]–[9]. Lithium niobite (LiNbO₃) and indium phosphide (InP) based modulators have mostly been used to demonstrate these results due to their superior electro-optic properties. However, bulk LiNbO₃ MZMs cannot be utilized in pluggable optical transceivers due to their larger footprint and neither InP nor LiNbO₃ based modulators are compatible with complementary metal-oxide-semiconductor (CMOS) foundries which hinder large-scale, low-cost production. Alternatively, hybrid integration of materials like polymers, thin-film lithium niobite, III-V semiconductors on silicon (Si) has been reported to combine the high electro-optic performance of other material platforms with the scalability of the already established CMOS process. But these designs require additional process, and thus cannot be entirely realized in a commercial silicon-on-insulator (SOI) process [10], [11]. Due to compatibility with the CMOS process, small footprint and cost-effectiveness, Silicon Photonics (SiP) has emerged as the most promising technology for massive deployment, and SiP modulators are now being extensively investigated both in IM/DD and coherent communication [12]–[17].

Most SiP modulators are based on carrier depletion traveling wave (TW) Mach-Zehnder or micro-ring resonator (MRM) structures [18]. Recent years have witnessed reports on high-speed IM/DD systems with SiP modulators targeting 200 Gbps. In [19], 200 Gbps PAM4 transmission using a silicon MRM was demonstrated at B2B in the O-band at a BER of 1.08×10^{-3} , which is the highest reported rate for a Si MRM. In [12],

200 Gbps PAM6 (net 167 Gbps) signal transmission over 1 km of SMF was achieved at a BER below the 20% HD-FEC threshold of 1.5×10^{-2} using a SiP TW-MZM with a 3-dB EO bandwidth of ~ 22.5 GHz and complex receiver DSP, which included post-filter and maximum likelihood sequence detector (MLSD). We have previously reported transmission of net 200 Gbps over 2 km of SMF in the O-band using a segmented-electrode MZM (SE-MZM) with 45 GHz 3-dB E-O bandwidth and simple linear feed forward equalization [20]. But this result required two drive signals with precise phase alignment making it challenging to control with practical RF delay lines. Most recently, we designed a high bandwidth single segment MZM with an on-chip termination (OCT) intentionally lower than the TW electrode characteristic impedance and demonstrated net 212.5 Gbps/ λ transmission in the O-band [21].

In this paper, we extend on this contribution by providing experimental characterizations of both C-band and O-band designs with two different phase shifter lengths. Moreover, we present improved performance using a Volterra nonlinear equalizer (VNLE) and probabilistic shaping (PS). We demonstrate in the O-band, net 220 Gbps transmission over 2 km with only linear equalization and a PS-PAM8 format and net 216 Gbps over 10 km with a VNLE and PAM8 modulation format using a 2.5 mm long phase shifter based MZM at the 20% overhead (OH) SD-FEC NGMI threshold of 0.8798. This modulator has a 3-dB bandwidth of 47 GHz and a bandwidth over V_π figure of merit (BW/V_π FOM) of 8.7 GHz/V at -2 V bias. The MZM with a smaller phase shifter length of 1.5 mm shows a 3-dB bandwidth of over 50 GHz and allows net data rate of 225 Gbps at B2B in the O-band. With the mirror C-band design and a longer MZM we successfully transmit 215 Gbps over 500 m at the SD-FEC threshold. To the best of our knowledge, these are the highest reported IM/DD transmission rates in both O-band and C-band using a SiP MZM, fabricated entirely in a commercial SOI process. The rest of this paper is organized as follows: in Section II, we present the small-signal responses of the designed modulators followed by the description of the experimental set-up and DSP algorithms for transmission experiment in Section III. In Section IV, we present our transmission experiment results in the O-band for different modulation formats and equalization schemes and in Section V, we focus on C-band transmission results. Finally, we discuss the main points, and we conclude in Section VI.

II. MODULATOR DESIGN AND CHARACTERIZATION

In this section, we describe the design and characterization of the TW-MZMs. The C-band and O-band modulator designs both adopt the series push-pull (SPP) configuration with a layout shown in Fig. 1, where the two PN junctions of each arm are connected back-to-back and a DC bias is applied to the common N++ region. This doubles the junction resistance and halves the junction capacitance [22]. The fabrication process admits a RF electrode design with two metal layers that reduces microwave attenuation. For each of the two optical bands, we have designed the MZM with two different phase-shifter lengths, 1.5 mm (S) and 2.5 mm (L). Both the O-band and C-band modulator

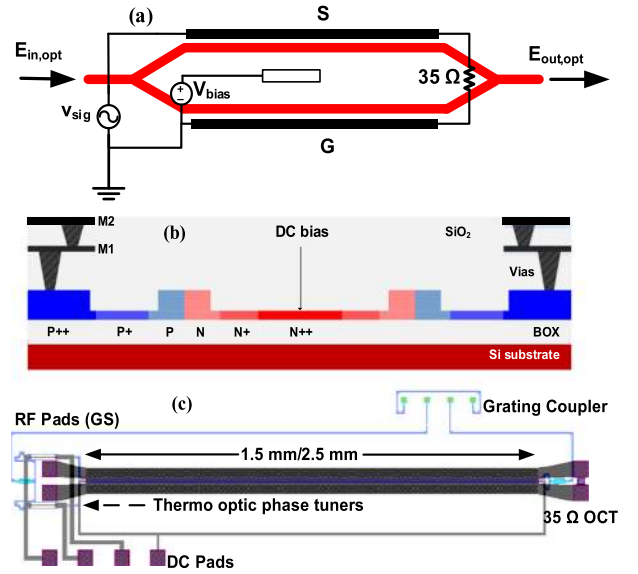


Fig. 1. (a) TW-MZM top-view schematic, (b) SPP-MZM cross-section. BOX: buried oxide, M1/M2: metal layers and (c) SPP-MZM layout.

designs use the same doping densities. The only difference lies on the optical waveguide width. The waveguide widths of the MZMs have been chosen to ensure single-mode operation and maximize optical field/carrier overlap. A reduced waveguide width is used for the O-band design for this reason. As these modulators are designed for high data rate links required by the intra-data center interconnects, we peak the device frequency response to obtain a higher E-O bandwidth by implementing a 35Ω on-chip termination (OCT), intentionally mismatched to the traveling-wave electrode characteristic impedance [23]. Vertical grating couplers (GC) are used for the optical input and output and the MZM operating point is set using thermal phase shifters.

Fig. 2 shows the E-O S_{21} and E-E S_{11} magnitude responses of the 2.5 mm C-band and O-band modulator. A 50 GHz Keysight lightwave component analyzer (LCA) and 50 GHz RF probes are used to perform the small-signal characterization. From Fig. 2, it can be observed that the RF return loss (S_{11}) is below 10 dB within the entire measurement spectrum. Also, the E-O S_{21} magnitude responses show that the 3-dB bandwidths of both C-band and O-band modulators are approximately 47 GHz at a 3V reverse bias (normalized to 1.5 GHz). This 3-dB bandwidth allows 100 Gbaud signaling for single-carrier 200 Gb/s links with simple linear FFE as will be shown in the following sections. The S_{21} magnitude responses of the MZMs with a shorter phase shifter length are not shown here but they have better bandwidth, at the expense of a higher V_π as shown in Table I [24]. From the E-O S_{21} frequency response curves, we can also see that there is a clear peaking at lower frequency (at around 12 GHz). As mentioned earlier, the gain peaking at this frequency comes due to the impedance mismatch between the traveling-wave electrode characteristic impedance of 50Ω and on-chip termination (OCT) of 35Ω . It acts like a pre-emphasis and extends the bandwidth of the modulators.

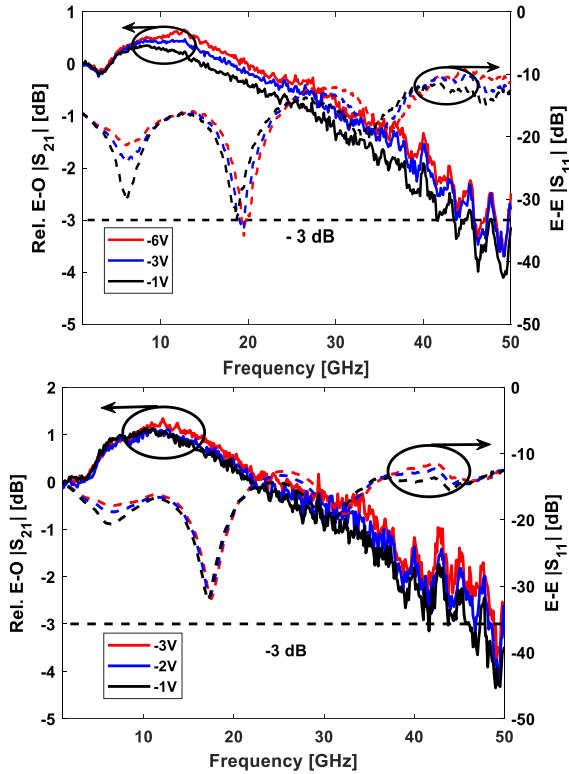


Fig. 2. Measured small-signal response of the MZMs ($E\text{-}O |S_{21}|$ is normalized to 1.5 GHz): C-band (L) MZM (top), and O-band (L) MZM (bottom).

TABLE I
O-BAND AND C-BAND MODULATORS AT -2 V BIAS

Metric	O-band MZM (S)	O-band MZM (L)	C-band MZM (L)
Phase shifter length (mm)	1.5	2.5	2.5
DC V_π (V)	6.6	5.4	7.6
-3dB E-O BW (GHz)	> 50	47	46
BW/ V_π (GHz/V)	> 7.5	8.7	5.9
Total opt. Propagation loss (dB)	4	5.4	8.4

Fig. 3 shows the DC transfer functions (TFs) of the 2.5 mm (L) O- and C-band modulators when differential voltages ($\pm V_{arm}$) are applied simultaneously through the DC needle probes to the ‘G’ and ‘S’ electrodes. Here, we show the DC transfer function in terms of normalized optical power. This normalization is done with respect to the maximum optical power received at 3V reverse bias voltage. As the optical propagation loss is reduced with the increase in the applied reverse bias voltage, we reach at slightly lower maximum normalized power at 1V reverse bias than at 3V reverse bias voltage. The V_π is then calculated as $V_\pi = V_{TF, max} - V_{TF, min}$, where $V_{TF, max} = V_{arm1} - V_{arm2}$ is the total bias voltage applied for the maximum power and $V_{TF, min}$ is the bias voltage required for the minimum power. This method yields a slightly smaller V_π than typical single-ended methods due to less severe PN

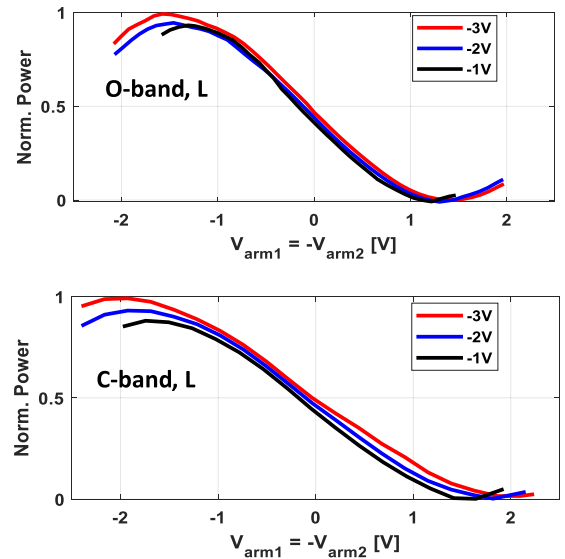


Fig. 3. Measured MZM DC transfer function at different DC bias voltage for the O- and C-band (L) MZM.

junction depletion width saturation. But this is closer to the actual operation of a SPP MZM. For the O-band modulator at 2V reverse bias, P_{max} is found at $V_{arm1} = -V_{arm2} = +1.35$ V and P_{min} at $V_{arm1} = -V_{arm2} = -1.35$ V. Thus, for this O-band design, $V_\pi = 5.4$ V whereas the C-band modulator yields a higher V_π of 7.6 V. The different phase shifting efficiency in O and C bands come from i) the different effective refractive index change, $\Delta n_{eff}(E)$ as a function of the applied voltage, which depends on the plasma dispersion effect and the overlap fraction between the optical mode and the free-carriers being modulated around the PN junction, and ii) the wavelength, λ at the denominator of the phase shifter equation, $\Delta\varphi = 2\pi\Delta n_{eff}(E)L/\lambda$, where L is the phase shifter length. For the same phase shifter length, these factors cause the V_π to be higher for the C-band modulator compared to the O-band one. The V_π of the C-band MZM becomes even higher at a shorter length of 1.5 mm, which requires high driving voltages that are challenging for practical transmitter RF chains and poses a high modulation power consumption, making it unsuitable in DCI scenario. Therefore, we will mainly discuss the transmission performance of three modulator designs with their key parameters summarized in Table I. The high optical propagation loss is due to a layout error (exaggerated proximity of P+ and N+ doped regions with the optical waveguide) and is worse in the C-band designs and will be corrected in future versions.

III. EXPERIMENTAL SET-UP AND DIGITAL SIGNAL PROCESSING

The experimental setup and DSP used to test the transmission performance of the designed modulators is shown in Fig. 4. The set of instruments used to test O-band and C-band modulators are the same except the laser and optical amplifier. In O-band experiment, 13 dBm of power is launched at 1302.8 nm which is then coupled to the chip using the grating coupler, whereas, in C-band, 15.25 dBm of power at 1550 nm is used as the CW

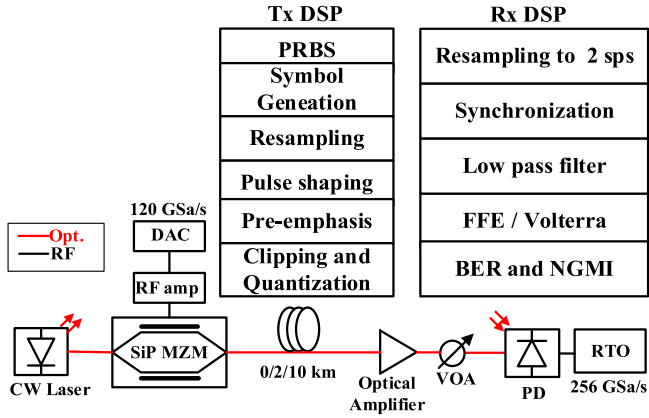


Fig. 4. Experimental set up and DSP deck.

light source. The measured back-to-back grating coupling loss is found to be 7.5 dB and 9.5 dB for the O-band and C-band grating couplers, respectively. This difference comes from a better GC design in the O-band case. DC probes are used to reverse bias the PN junction of the modulator and tune the thermal shifters. At the transmitter, a PRBS sequence is generated and then mapped to PAM symbols. After resampling the symbols to the DAC sampling rate, pulse shaping is done via a raised cosine (RC) filter. Next, a pre-emphasis filter pre-compensates for the low pass filtering of the DAC and RF amplifier. Note that, we do not use any non-linearity pre-compensation for the MZM. The digital signal is then clipped, quantized and loaded to a 120 GSa/s 8-bit digital-to-analog converter (DAC). The DAC output is amplified by an RF amplifier with 45 GHz 3-dB bandwidth and 26-dB gain and then applied to the modulator using 50 GHz RF probes. As the pre-emphasis filter flattens the entire transmitter RF chain including the RF amplifier, the lower bandwidth of the amplifier compared to the devices under test do not limit the system performance in terms of bandwidth. To test the transmission performance, we adopt different PAM formats from 65 Gbaud to 110 Gbaud and the roll-off factor is empirically optimized at these different symbol rates.

After the modulator, the optical signal is transmitted over various distances of standard single-mode fiber (SSMF). To compensate for the grating coupler loss and modulator optical loss, a praseodymium-doped fiber amplifier (PDFA) or an Erbium-doped fiber amplifier (EDFA) is used to provide sufficient received optical power (ROP) to the 50 GHz PIN photodetector (PD). The noise figure of the PDFA and EDFA used is 6.5 dB and 5 dB, respectively. A variable optical attenuator (VOA) is added before the PD to control the ROP. The signal out of the PD is then digitized by a real time oscilloscope (RTO) with a bandwidth of 110 GHz operating at 256 GS/s. As the transmitter signal bandwidth is kept within 60 GHz, the RTO bandwidth is set to 63 GHz so that out of band noise is filtered automatically. Finally, the signal is processed offline by the receiver DSP, which includes re-sampling to 2 sps, synchronization, linear feed-forward equalization (FFE) or Volterra non-linear equalization (VNLE), symbol de-mapping

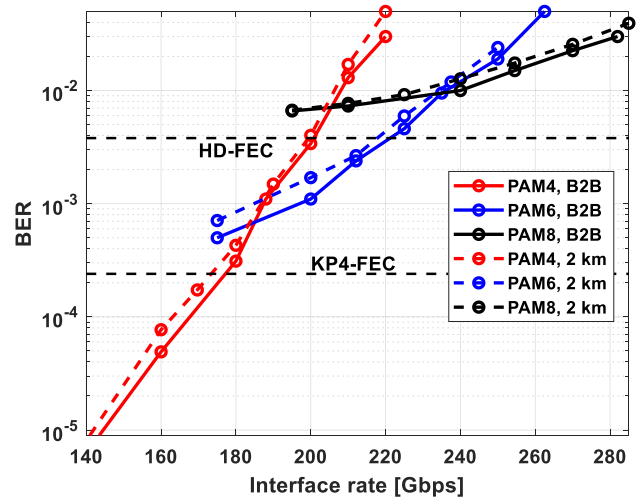


Fig. 5. BER versus interface rate for PAM4, PAM6, and PAM8 at B2B and 2 km with FFE.

and bit-error ratio (BER) counting and normalized generalized mutual information (NGMI) computing.

IV. O-BAND TRANSMISSION EXPERIMENT RESULTS

A. PAM Transmission Results With Linear Equalization

In this section, we investigate the transmission performance of the O-band 2.5 mm MZM, which has the maximum phase-shifting efficiency among the designs. A reverse bias voltage of 2 V is used, which gives the best performance for this longer modulator. This also ensures >45 GHz 3-dB bandwidth which is useful when operating at high symbol rates. At the MZM quad point, the power out of the chip is around -4 dBm, which is then launched into the SMF. The peak-to-peak driving voltage after the RF amplifier depends on the symbol rate, roll-off factor, and clipping ratio. The maximum peak-to-peak voltage, V_{pp} that we drive the modulator with is 2.6 V_{pp} and 2.3 V_{pp} at 85 Gbaud and 90 Gbaud respectively.

Fig. 5 shows the BER versus interface rate at B2B and after 2 km of SMF for different PAM formats. The received optical power is set to 8.5 dBm and only linear FFE is used in the receiver signal processing. The red curves represent PAM4 BER as the symbol rate is varied from 70 Gbaud to 110 Gbaud. The figure shows that we can achieve 170 Gbps and 200 Gbps interface rate PAM4 transmission over 2 km of SMF at a BER below the KP4-FEC threshold and 6.7% HD-FEC threshold, respectively. However, net 200 Gbps (214 Gbps interface rate assuming HD-FEC) with PAM4 format is not achievable due to the limited bandwidth of the system. The blue curves in Fig. 5 show the BER of the PAM6 format. Here, PAM6 symbols are generated from a 32-QAM 2D constellation which maps five bits into two symbols with a spectral efficiency of 2.5 bits/symbol [25]. We sweep the symbol rate for PAM6 format ($= 70 \times 2.5$ Gbps = 175 Gbps interface rate) to 105 Gbaud (262.5 Gbps interface rate). 218 Gbps PAM6, which corresponds

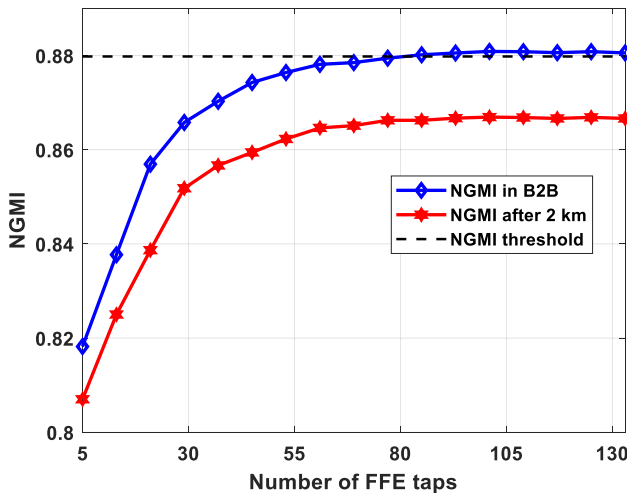


Fig. 6. NGMI vs number of FFE taps for a 90 Gbaud PAM8 signal.

to a throughput of 203 Gbps is achieved with this modulator design below the HD-FEC threshold after 2 km propagation.

The PAM8 format has a higher SNR requirement and cannot achieve a throughput of interest (>200 Gbps) at the HD-FEC. Therefore, to evaluate the system performance, we adopt a practical SD-FEC coding scheme where spatially coupled low-density parity-check code (code rate of 0.8469) is concatenated with an outer hard-decision, BCH code (8191,8126,5) [26] and compute the NGMI as a more precise metric to evaluate the transmission performance [27]. The combined FEC code rate is 0.8402, and the NGMI threshold is 0.8798. Here, we calculate the NGMI as: $NGMI(X; Y) = 1 - (H(X) - GMI(X; Y))/m$, where Y and X are the received and transmitted symbols, respectively, $H(X)$ is the entropy of the transmitted symbols, m is the number of bits used for each symbol based on the binary-reflected Gray code. GMI is calculated based on the log-likelihood ratios (LLRs). In Fig. 6 we show the calculated NGMI of a 90 Gbaud PAM8 signal (225 Gbps net data rate) as we sweep the number of FFE taps. We find that a minimum of 81 taps are required for an NGMI above the threshold of 0.8798 at B2B. However, this is not achievable for the case of 2 km regardless of the number of taps used. We show in the following section that by mitigating the nonlinearity using the Volterra nonlinear equalization we can achieve 225 Gbps net data rate PAM8 transmission over 2 km.

B. PAM Transmission Results With Nonlinear Equalization

At a transmission reach of 2 km, the non-linearity of the system primarily comes from the system components, rather than the optical fiber. One source of these impairments is the non-linear phase shifter of the SiP modulator. Also, to keep a reasonably high driving voltage swing into the modulator at high symbol rates, we clip the signal before loading it into the DAC, which also introduces non-linearity into the signal. Nonlinear equalization has been shown to be effective in improving system performance even in optical short reach scenarios [28], [29].

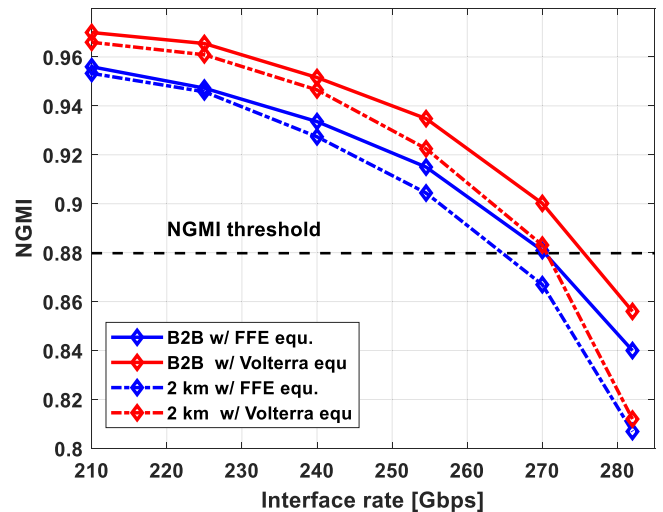


Fig. 7. NGMI vs interface rate for PAM8 signals with linear and non-linear equalization.

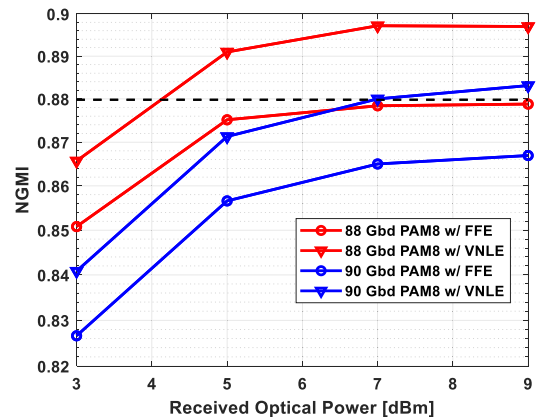


Fig. 8. NGMI vs ROP after 2 km transmission with FFE and VNLE.

Fig. 7 plots the NGMI vs interface rate using the PAM8 modulation format. We find that second order VNLE enables the transmission of a 90 Gbaud (270 Gbps) PAM8 signal with an NGMI above the threshold, which corresponds to net 225 Gbps, over 2 km of SMF. For these results a second order Volterra equalizer at 2 samples per symbol is used. The memory lengths for the linear terms and the nonlinear terms of second order Volterra equalizer is chosen to be 61 and 7 respectively. The performance improvement is not significant for higher memory lengths. Thus, we use these memory lengths for the rest of the results with the VNLE. In Fig. 8, we show the NGMI as we sweep the received optical power for 88 and 90 Gbaud PAM8 signals. These figures show that second order VNLE allows the throughput of PAM8 format to extend by 5 Gbps only. Due to the low driving voltage swing into the modulator, we operate mostly in the linear region of modulator, leading to little non-linear effect from the modulator side. Third order Volterra equalizer do not show significant improvement as well and considering its complexity we do not employ it in our results. Fig. 8 also shows that the minimum required ROP for net 220 Gbps and 225 Gbps

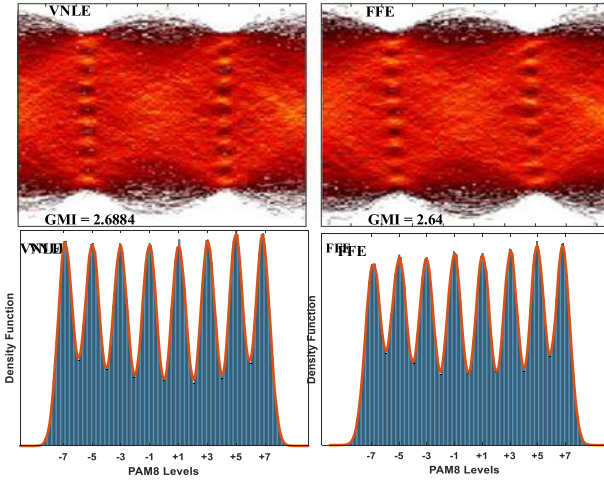


Fig. 9. Eye diagram and histogram of 90 Gbaud PAM8 signal with receiver VNLE and FFE at B2B.

after 2 km transmission is 4.1 dBm and 7 dBm, respectively. Here we use PDFA followed by a VOA to sweep the ROP while the launch power is kept at -4 dBm. We also test the impact of the VNLE for PAM4 and PAM6 modulation formats. Unlike PAM8, the performance improvement is not that pronounced. This is primarily because of the smaller number of inner levels for these formats.

In Fig. 9, we draw the eye-diagram of the net 225 Gbps B2B signal with and without nonlinear equalization. We find that in both cases the outermost eyes are more closed than the inner eyes. The histogram of the received symbols shows that the outermost levels are less separated from each other than the inner levels and cause more errors. We can also see that the levels are more distinguishable at the decision thresholds using nonlinear equalization (VNLE) than linear FFE. Probabilistic shaping can improve the system performance as the outer levels are transmitted with lower probability thus improving the BER performance. However, PS-PAM8 will require higher symbol rate transmission for the same throughput and an optimum choice is to be made.

C. PAS PAM Transmission Results

The use of standard PAM formats results in a coarse grid of spectral efficiency (SE) as well as the corresponding symbol rates required at each SE to achieve net 200 Gbps data rate. For example, PAM4 signaling requires the system to operate at 107 Gbaud assuming a 6.7% HD-FEC, which poses a stringent requirement on the system bandwidth. On the other hand, PAM8 signaling is demanding on the system SNR due to limited effective number of bits (ENoB) of the DAC and ADC. Thus, to improve the system throughput, it is desirable to transmit probabilistic shaped signals with a finer SE granularity so that we can best exploit the trade-off between inter-symbol interference (ISI) and system SNR. In this paper, we use cost-minimizing distribution matching (CMDM) within the probabilistic amplitude shaping (PAS) scheme to generate PS-PAM8 signals with varied

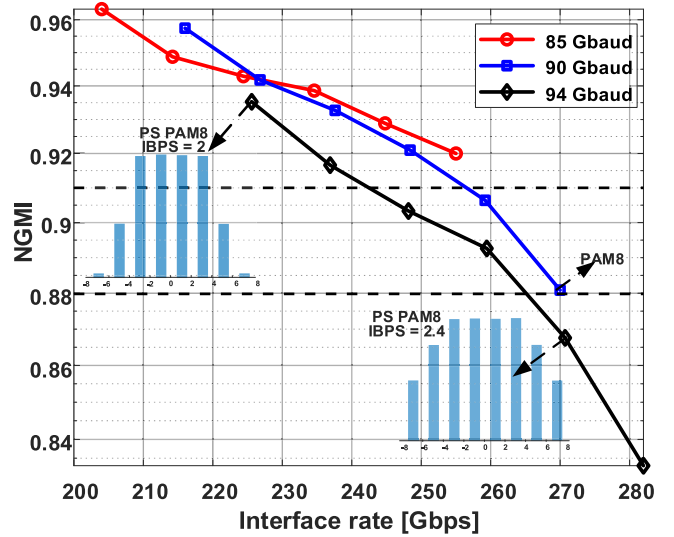


Fig. 10. NGMI versus interface rate for PS-PAM8 signals with varied IBPS at three symbol rates at B2B.

SEs. CMDM is implemented by means of a lookup-table (LUT) [30], where a varied number of bits from 13 to 19 are mapped to a block of 10 symbols and provides a tunable information bit per symbol (IBPS) from 1.8 to 2.4 bits/symbol assuming 20% FEC overhead. Since the weight of the symbol sequences are set as the sequence power, the PS-PAM8 symbols approach the Maxwell-Boltzmann distribution.

In Fig. 10, we show the NGMI of PS-PAM8 signals with varied IBPS at three different symbol rates at B2B. Note that only linear equalization is used at the receiver. We sweep the IBPS from 2 to 2.5 bits/symbol, which means for 90 Gbaud PS-PAM8 signals, we can tune the net throughput from 180 Gbps to 225 Gbps with a step of 9 Gbps. The histogram of the transmitted symbols for two different IBPS values is also shown in the inset. As the IBPS increases, the transmitted signal become more and more identical to a uniform PAM8 signal, which corresponds to an IBPS of 2.5 ($= 3/1.2$) bits/symbol. We can also see that the 94 Gbaud PS-PAM8 signal shows notably worse performance than the 90 Gbaud and 85 Gbaud signals at the same interface rate. This result is attributed to a stronger ISI increase and voltage swing decrease as the signal bandwidth exceeds the system bandwidth. At this high symbol rate of 94 Gbaud, stronger pre-emphasis and smaller roll-off factor is used such that the signal PAPR increases sharply and thus the driving signal swing decreases, which degrades the transmitted signal SNR and decreases the modulation depth. The performance difference between the 90 Gbaud and 85 Gbaud signals, on the other hand, is relatively moderate since the roll-off of the system response degrades more slowly within the system bandwidth of 45 GHz. The optimum choice of the symbol rate and the IBPS depends on the trade-off between the induced ISI and the system SNR. For our system, the NGMI of the 85 Gbaud signal shows slightly higher NGMI than the 90 Gbaud signal for interface rates beyond 225 Gbps. Thus, at each desired throughput, the symbol rate and IBPS need to be appropriately determined.

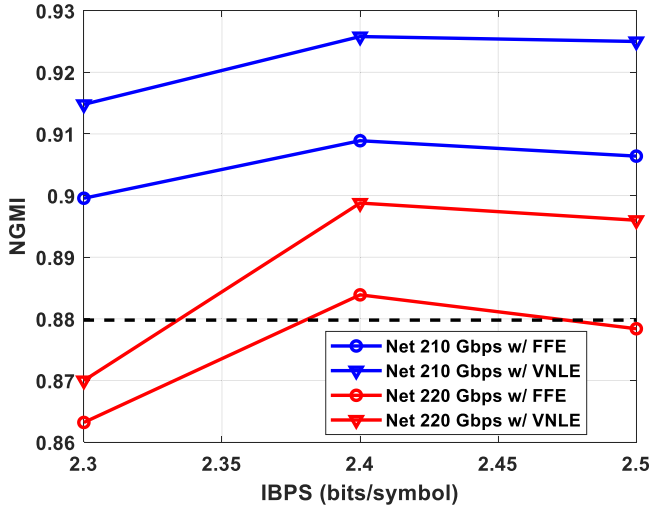


Fig. 11. NGMI versus IBPS for net 210 Gbps and 220 Gbps after 2 km.

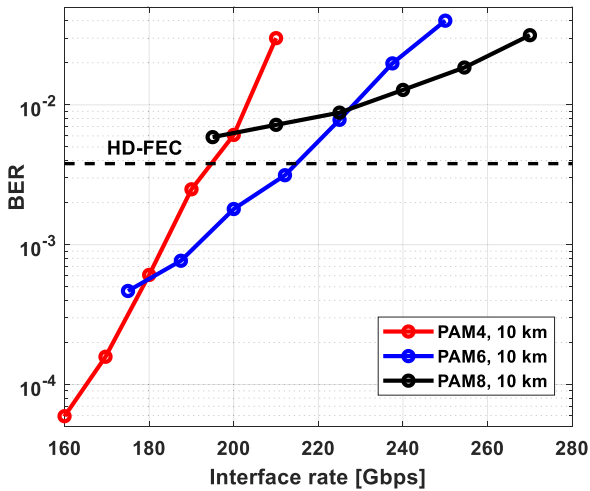


Fig. 12. BER vs interface rate after 10 km transmission.

Next, we try to find the IBPS that achieves the highest NGMI at a target net data rate for our system after 2 km propagation with linear and non-linear equalization. The blue and red curves in Fig. 11 show the NGMI values at different symbol rates and corresponding SEs for net 210 Gbps and net 220 Gbps, respectively. We can see that PS-PAM8 with an IBPS of 2.4 bits/symbol delivers the highest NGMI for these net rates for both linear and non-linear equalization. Lower IBPS (2.3) at a high symbol rate is not a good choice because of stronger ISI and lower driving voltage swing. For net 220 Gbps with linear FFE, only 2.4 bits/symbol PS-PAM8 at 91.6 Gbaud is found above the NGMI threshold and outperforms uniform PAM8 signaling.

D. 10 km PAM Transmission Results

10 km transmission is important for LR (long reach) datacenter interconnects and Fig. 12 shows the BER performance over 10 km of SMF with different modulation formats and receiver VNLE. We can see that using PAM6 format, we can transmit

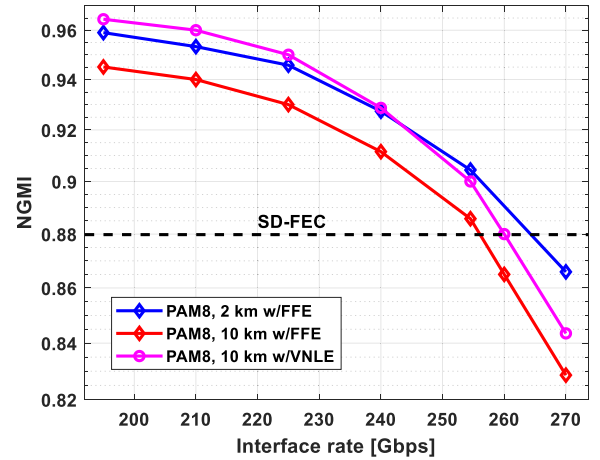


Fig. 13. NGMI vs interface rate with PAM8 format.

TABLE II
MZM BER PERFORMANCE FOR SHORT AND LONG MODULATOR

Modulation Format	Short MZM	Long MZM
100 Gbaud PAM4 (200 Gbps)	5e-3	3.4e-3
90 Gbaud PAM6 (225 Gbps)	4e-3	3.2e-3

net 200 Gbps (interface rate of 214 Gbps) below the HD-FEC threshold. In Fig. 13, we show the achievable NGMI for PAM8 format with linear and nonlinear equalization schemes. The 2 km curve with linear equalization is also added here for comparison. The maximum achievable throughput after 10 km of SMF is 216 Gbps, achieved with 86 Gbaud PAM8 format and VNLE. Like 2 km results, the NGMI gain with VNLE is not significant, meaning the nonlinear degradation is not that severe for 10 km transmission as well.

Fig. 13 also shows that compared to 2 km transmission, the results are slightly worse for the 10 km case. The effect of dispersion is negligible over 10 km of SMF at our wavelength of operation (1302.8 nm). Therefore, the degradation comes mostly from the reduced OSNR of the received signal. As mentioned earlier, the launch power into the fiber is -4 dBm and after 10 km transmission this becomes -7.5 dBm, which is then amplified via the PDFA. But the lower input power into the PDFA increases the noise figure (NF) and worsens the signal OSNR. Considering short reach application scenario, PDFA is not a viable solution and better light coupling in this case would increase the launch power into the fiber, thereby improving the transmission performance.

E. Experiment Results for Shorter MZM

Next, we focus on the shorter MZM with a phase shifter length of 1.5 mm. This modulator has a 3 dB E-O bandwidth of over 50 GHz and a lower optical propagation loss, but this comes at the expense of a higher V_{π} . The optimized reverse bias voltage for this modulator is found to be 0.5 V. From Table II and Fig. 14, we find that despite the higher E-O bandwidth, the shorter MZM

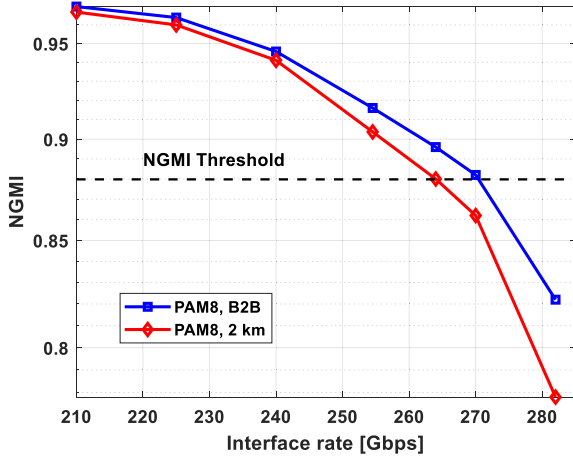


Fig. 14. NGMI versus interface rate with PAM8 format for shorter MZM.

shows worse transmission performance compared to the longer one for all formats. Fig. 14 plots the NGMI versus interface rate with this MZM at B2B and after 2 km propagation with a VNLE. The shorter MZM achieves 270 Gbps PAM8 (net 225 Gbps) at the B2B scenario and after 2 km, the highest interface rate that is above the NGMI threshold is 264 Gbps, corresponding to a throughput of 220 Gbps. As the roll-off factor chosen for the 90 Gbaud signal is 0.1, the one-sided signal bandwidth is 49.5 GHz. Therefore, the higher E-O bandwidth of the shorter MZM does not improve the performance significantly, rather the higher V_{π} decreases the modulation depth of the transmitted signal and causes the overall results to degrade. Even at higher symbol rate operation, this modulator shows worse performance. But the total footprint of this modulator is $0.9 \text{ mm} \times 2.2 \text{ mm}$, as compared to the longer one with $0.9 \text{ mm} \times 3.2 \text{ mm}$ footprint, which makes it good choice if space is an important factor.

V. C-BAND TRANSMISSION EXPERIMENT RESULTS

In this section, we present the transmission results using the C-band modulator. As shown is Table I, the C-band modulator has a much higher V_{π} as compared to the O-band design. Based on the previous explanations, we choose the modulator with the longer phase shifter length (2.5 mm) for a better phase shifter efficiency. In Fig. 15, we show the BER of PAM4 and PAM6 format and NGMI of PAM8 signaling at different interface rates. The B2B BER for 100 Gbaud signaling is found to be $8.5e-3$, which is worse than the O-band designs because of its higher V_{π} . Net 200 Gbps below the HD-FEC threshold is still achievable using 86 Gbaud PAM6 at B2B. After 500 m the maximum throughput below the HD-FEC threshold is 195 Gbps at 84 Gbaud with PAM6 format. For PAM8 signaling, at B2B maximum 264 Gbps (net 220 Gbps) is achievable above the NGMI threshold and for a 500 m transmission, it is reduced to 258 Gbps (net 216 Gbps). For 2 km reach, the signal is heavily affected due to dispersion induced power fading which is clear from the received electrical spectrum of the 85 Gbaud signal shown in Fig. 16. 72 Gbaud PAM8, which is equivalent to a net 180 Gbps signal can

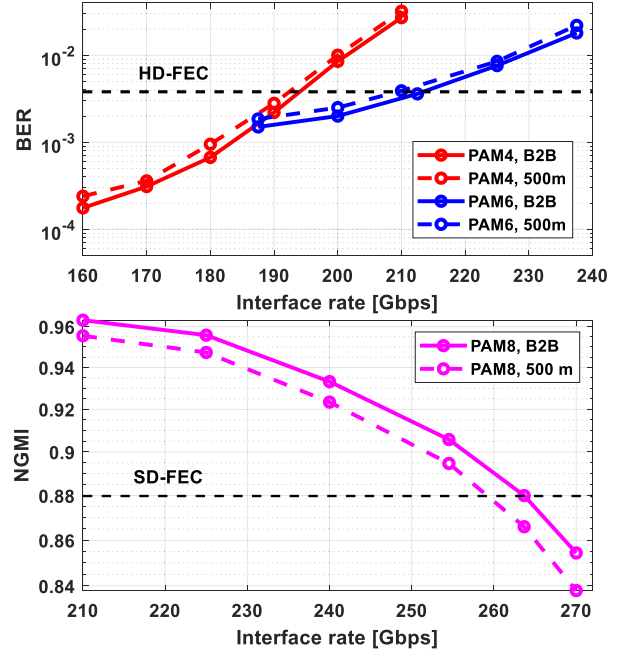


Fig. 15. BER (top) and NGMI (bottom) vs interface rate for C-band MZM.

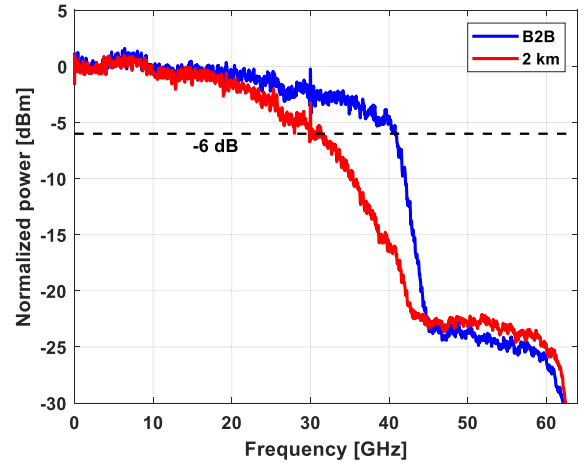


Fig. 16. Received electrical spectrum at B2B and after 2 km for 85 Gbaud signal.

be transmitted over 2 km of SMF using receiver VNLE at the SD-FEC threshold.

VI. DISCUSSION AND CONCLUSION

In this manuscript, we report the small-signal, and large-signal characterization of high bandwidth SiP MZM modulators. It is found that besides the importance of a high E-O bandwidth, the transmitter driving voltage and modulator V_{π} are also key factors which determines system performance. Since meeting the low power consumption constraint in data centers necessitates a low driving power, modulator designs with optimized phase shifting efficiency is preferable. In our case, the modulator with the longer phase shifter has lower V_{π} compared to the design

with shorter phase shifter, and thus delivers better transmission performance despite a slightly lower E-O bandwidth of 47 GHz. This modulator design enables 100 Gbaud PAM4 signal transmission below the 7% HD-FEC threshold with only linear FFE. Since it is desirable to use high code rate HD-FEC for real-time short reach systems with a high throughput decoder, PAM6 seems to be an attractive signal format to attain net 200 Gbps and works as a compromise between PAM4 and PAM8 modulation formats in terms of the system bandwidth and SNR requirement. Our results also show that higher order formats such as PAM8 or PS-PAM8 allow higher throughput at the expense of higher overhead SD-FEC. Considering the power constraint of transceivers used within the data centers, nonlinear equalizers are not preferred and depending on the system non-linearity, reduced-complexity Volterra equalizers [31] or look-up-table (LUT) based nonlinear pre-distortion schemes [32] might be adopted, and short block length distribution matchers such as CMDM can be utilized to facilitate the high-speed parallel signal processing.

Using our best modulator designs with over 45 GHz 3-dB E-O bandwidth, we transmit net 225 Gbps PAM8 signaling over 2 km of SMF in the O-band and net 215 Gbps over 500 m of SMF in the C-band above the 20% overhead SD-FEC NGMI threshold. These are the highest reported IM/DD transmission rates using a SiP modulator which shows great potential for single lane 200 G intra-data center applications.

REFERENCES

- [1] Cisco Global Cloud Index: Forecast and Methodology, 2017-2022 White Paper.
- [2] *Ethernet Amendment 10: Media Access Control Parameters, Physical Layers, and Management Parameters for 200 Gbps and 400 Gbps Operation*, IEEE Standard 802.3bs, 2017.
- [3] QSFP-DD Multi-source Agreement Specification. [Online]. Available: <http://www.qsfp-dd800.com/>
- [4] X. Pang *et al.*, "200 Gbps/Lane IM/DD technologies for short reach optical interconnects," *J. Lightw. Technol.*, vol. 38, no. 2, pp. 492–503, Jan. 2020.
- [5] C. Wang *et al.*, "100-GHz low voltage integrated lithium niobate modulators," in *Proc. Conf. Lasers Electron. Opt.*, 2018, Paper SM3B.4.
- [6] O. Ozolins *et al.*, "100 GHz externally modulated laser for optical interconnects," *J. Lightw. Technol.*, vol. 35, no. 6, pp. 1174–1179, 2017.
- [7] S. Kanazawa *et al.*, "Transmission of 214-Gbps 4-PAM signal using an ultra-broadband lumped-electrode EA DFB laser module," in *Proc. Opt. Fiber Commun.*, 2016, Paper Th5B.3.
- [8] T. Wettlin *et al.*, "Comparison of PAM formats for 200 Gbps short reach transmission systems," in *Proc. Opt. Fiber Commun.*, 2020, Paper Th2A.37.
- [9] S. Lange *et al.*, "100 GBd intensity modulation and direct detection with an InP-based monolithic DFB laser Mach-Zehnder modulator," in *Proc. Opt. Fiber Commun.*, 2017, Paper Th5C.5.
- [10] C. Kieninger *et al.*, "Ultra-high electro-optic activity demonstrated in a silicon organic hybrid modulator," *Optica*, vol. 5, no. 6, pp. 739–748, 2018.
- [11] P. O. Weigel *et al.*, "Bonded thin film lithium niobate modulator on a silicon photonics platform exceeding 100 GHz 3-dB electrical modulation bandwidth," *Opt. Exp.*, vol. 26, no. 18, pp. 23728–23739, 2018.
- [12] Y. Zhu *et al.*, "Toward single lane 200G optical interconnects with silicon photonic modulator," *J. Lightw. Technol.*, vol. 38, no. 1, pp. 67–74, 2019.
- [13] H. Zhang *et al.*, "800 Gbps transmission over 1 km single-mode fiber using a four-channel silicon photonic transmitter," *Photon. Res.*, vol. 8, no. 11, pp. 1776–1782, 2020.
- [14] J. Zhou, J. Wang, L. Zhu, and Q. Zhang, "High baud rate all-silicon photonics carrier depletion modulators," *J. Lightw. Technol.*, vol. 38, no. 2, pp. 272–281, 2020.
- [15] A. Samani *et al.*, "Silicon photonic Mach-Zehnder modulator architectures for on chip PAM-4 signal generation," *J. Lightw. Technol.*, vol. 37, no. 13, pp. 2989–2999, Jul. 2019.
- [16] M. Li *et al.*, "Silicon intensity Mach-Zehnder modulator for single lane 100 Gb/s applications," *Photon. Res.*, vol. 6, no. 2, pp. 109–116, 2018.
- [17] A. Samani *et al.*, "A low-voltage 35-GHz silicon photonic modulator-enabled 112-Gb/s transmission system," *IEEE Photon. J.*, vol. 7, no. 3, pp. 1–13, 2015.
- [18] W. Shi *et al.*, "Silicon photonic modulators for PAM transmissions," *J. Opt.*, vol. 20, no. 8, 2018, Art. no. 083002.
- [19] Y. Zhang *et al.*, "200 Gbit/s optical PAM4 modulation based on silicon microring modulator," in *Proc. Eur. Conf. Opt. Commun.*, 2020, Paper Th3A.1.
- [20] M. Jacques *et al.*, "200 Gbps net rate transmission over 2 km with a silicon photonic segmented mZM," in *Proc. Eur. Conf. Opt. Commun.*, 2019, Paper PD.1.6.
- [21] M. Jacques *et al.*, "Net 212.5 Gbps transmission in O-band with a SiP MZM, one driver, and linear equalization," in *Proc. Opt. Fiber Commun.*, 2020, Paper Th4A.3.
- [22] D. Patel *et al.*, "Design, analysis, and transmission system performance of a 41 GHz silicon photonic modulator," *Opt. Exp.*, vol. 23, no. 11, pp. 14263–14287, 2015.
- [23] H. Yu and W. Bogaerts, "An equivalent circuit model of the traveling wave electrode for carrier-depletion-based silicon optical modulators," *J. Lightw. Technol.*, vol. 30, no. 11, pp. 1602–1609, 2012.
- [24] D. Petousi *et al.*, "Analysis of optical and electrical tradeoffs of traveling-wave depletion-type Si Mach-Zehnder modulators for high-speed operation," *IEEE J. Sel. Top. Quantum Electron.*, vol. 21, no. 4, pp. 199–206, Jul./Aug. 2015.
- [25] N. Stojanovic *et al.*, "210/225 Gbps PAM-6 transmission with BER below KP4-FEC/EFEC and at least 14 dB link budget," in *Proc. Eur. Conf. Opt. Commun.*, 2018, pp. 1–3, doi: 10.1109/ECOC.2018.8535246.
- [26] J. Cho and L. Schmalen, "Construction of protographs for large-girth structured LDPC convolutional codes," in *Proc. IEEE Int. Conf. Commun.*, 2015, pp. 4412–4417.
- [27] A. Alvarado *et al.*, "Replacing the soft-decision FEC limit paradigm in the design of optical communication systems," *J. Lightw. Technol.*, vol. 33, no. 2, pp. 4338–4352, 2015.
- [28] L. Zhang *et al.*, "Kernel affine projection for nonlinearity tolerant optical short reach systems," *IEEE Trans. Commun.*, vol. 68, no. 10, pp. 6403–6412, 2020.
- [29] N. Stojanovic, F. Karinou, Z. Qiang, and C. Prodaniuc, "Volterra and Wiener equalizers for short-reach 100G PAM-4 applications," *J. Lightw. Technol.*, vol. 35, no. 21, pp. 4583–4594, 2017.
- [30] X. Li *et al.*, "Cost-minimizing distribution matching supporting net 800 gbps PS-PAM transmission over 2 km using a 4- λ EML TOSA," *Opt. Lett.*, vol. 45, no. 17, pp. 4718–4721, 2020.
- [31] N. Diamantopoulos, H. Nishi, W. Kobayashi, and K. Takeda, "On the complexity reduction of the second-order Volterra nonlinear equalizer for IM/DD systems," *J. Lightw. Technol.*, vol. 37, no. 4, pp. 1214–1224, Feb. 2019.
- [32] J. Zhang *et al.*, "PAM-8 IM/DD transmission based on modified lookup table nonlinear pre-distortion," *IEEE Photon. J.*, vol. 10, no. 3, Jun. 2018, Art. no. 7903709.